Spectroscopic study of self-pulsing discharge with liquid electrode

Goran B. Sretenović[1,2,*], Mubbshir Saleem[2], Omar Biondo[2], Giulia Tomei[2], Ester Marotta[2], Cristina Paradisi[2]

[1] University of Belgrade, Faculty of Physics, PO Box 44, 11001 Belgrade, Serbia
[2] Department of Chemical Sciences, University of Padova, Via Marzolo 1, 35131 Padova, Italy
* sretenovic@ff.bg.ac.rs

Abstract

The article is devoted to the spectroscopic investigation of the self-pulsing electrical discharge in contact with aqueous media. The discharge occurs between a bare high voltage electrode positioned over the liquid and a grounded ring submerged by the liquid. It is supplied with DC high voltage, but it operates in pulse mode that is determined by the charging and discharging of a parallelly connected capacitor. This type of discharge has attracted our attention due to its complex physics, as well as to its high efficiency in the degradation of highly inert hazardous pollutants, such as perfluoroalkyl substances. The generated discharge unites several types of plasma in a single discharge cell. It starts as a high temperature (2500 K), high electron density ($10^{16\text{-}17}$ cm^{-3}) spark-like discharge close to the high voltage electrode, then it branches into a large number of cooler leaders with one order of magnitude lower electron density (10^{15} cm^{-3}), in the middle of the gap and finally it touches the liquid electrode through a dense network of low temperature (500 K) and low electron density streamers (10^{14} cm^{-3}). The paper discusses the results of a parametric study which has provided data of temperature and electron density in different regions of the discharge under various experimental conditions which are relevant for applications in water decontaminating treatments. The measurements were thus performed for discharges in ambient air, in N_2/O_2 mixture and in argon, with, as liquid electrode, either tap or ultrapure (Milli-Q) water containing a small amount of perfluorooctanoic acid.

INTRODUCTION

Electrical discharges in and in contact with liquids are the focus of a broad and interdisciplinary field of research.[1,2] They have been attracting attention for a long time due to their unlimited application potential. The most studied field is application of plasma for degradation of chemical compounds and sterilization for water purification. Plasma is used for the removal of dyes[3,4], phenols[5,6], a wide range of medicaments[7,8], pesticides[9,10] and microorganisms[11]. In these studies, degradation efficiency measurements and chemical analysis of the treatment products are combined with investigations to characterize the discharge, in order to determine the main plasma-liquid interaction mechanisms and use this knowledge to optimize the process.

The discharge configuration investigated in this work was developed for perfluoroalkyl substances[12] (PFAS) decomposition and has already shown promising performance.[13] Degradation of artificial and resistant PFAS is one of the hot and most challenging topics the plasma community is being tackling since a few years.[13–20] This is due to the very stable chemical structure of PFAS that don't degrade in the environment, diffuse pervasively in soil and ground water and are taken

up by living organisms.[21] According to epidemiological studies, these hazardous compounds, which are present in 97% of American citizens[22], are probably responsible for a high incidence of thyroid disease, high cholesterol, ulcerative colitis, pregnancy-induced hypertension and also kidney and testicular cancers.[23,24] The study of PFAS degradation requires detection and quantification of the original pollutants, of their intermediates and final products, including their toxicity, accompanied by complete physical and chemical diagnostics of the discharge activated process. Further, optimization of these processes requires detailed discharge diagnostics. This article presents and discusses the results of a spectroscopic study of the discharge. The general features of this unique, so called self-pulsing discharge, have been determined for the conditions typically used for PFAS treatment and in its presence. Specifically, the work covers all experimental conditions tested in our previous article, which comparatively examined the process efficiency under different experimental settings.[13] The obtained data, such as temperatures and electron densities, will guide further optimization of the degradation processes.

EXPERIMENTAL SETUP

The discharge studied in this article is self-pulsing discharge (SPD) developed to treat PFAS contaminated water.[13] The basic electrode geometry is pin-to-ring. The tip of the high voltage pin electrode is placed above the liquid surface whereas the grounded ring electrode is submerged into the liquid, see Figure 1. The electrode system is placed in a 4 mm thick Pyrex cylinder with an internal diameter of 41 mm, a depth of 60 mm and a volume of 80 mL, forming a chemical reactor for treatment of liquid solutions. The reactor is closed with a cover made in Teflon and fitted with a Viton O-ring to make it airtight. The cover has a central port through which the high voltage electrode is inserted into the reactor, and two additional ports for gas inlet and outlet. The high voltage electrode is a 2 mm diameter rod in stainless steel, with a pointed tip reaching 3 mm above the liquid surface. A grounded steel ring (36 mm internal diameter and 2 mm thick) electrode was placed at the bottom of the reactor 8 mm below the liquid surface. Continuous mixing of the solution was provided by a magnetic stirring bar operated by placing the reactor over a magnetic stirrer. The discharge was operated in static ambient air, or in an 80.0/20.0 N_2/O_2 mixture denoted as “synthetic air”, or in argon. Synthetic air and argon experiments were performed in the flow regime with a constant flow of 100 mL min^{-1}. The liquid medium used in the experiments was either tap water or ultrapure (Milli-Q) water always in the presence of perfluorooctanoic acid (PFOA) at an initial concentration of 41.4 mg L^{-1}, 10^{-4} M. A set of six experiments, as detailed further, was performed for all possible combinations of working gas and liquid, to match the experiments performed in our previous study.[13] The pin electrode was powered by negative high voltage using a Spellman PTV30*350 (30 kV, 12 mA) high voltage power supply with the negative voltage polarity. The power supply was protected by a 2.5 MΩ high voltage resistor connected in series. A high voltage capacitor with the capacity of 3 nF was connected in parallel to the plasma reactor. The discharge operated in a self-pulsing discharge mode, thus the energy dissipated through the reactor was determined by the capacitor connected in parallel, see Figure 1. The electrical properties were determined by a Tektronix TDS5032B oscilloscope (350 MHz, 5 GS/s). Voltage signals were recorded using a Tektronix P6015A high voltage probe. Current was measured utilizing the standard voltage probe and a noninductive resistor of 3.3 Ω connected between the grounded electrode and the grounding point. The pulse frequency was kept

at 100 Hz for all experiments, by regulation of the HV power supply current i.e. the capacitor charging current. Besides the electrode geometry and the power supply, the discharge characteristics are determined also by the working gas and by the liquid conductivity which was measured by aMetrohm 660 Conductometer.

Spectroscopic measurements were performed with an optical system consisting of a spectrograph, a ccd detector and an optical fiber with focusing lens. The spectrograph was a Princeton Instruments Acton SP-2558 equipped with two gratings: UV adopted grating with 2400 g/mm and grating blazed at 500 nm with 1800 g/mm. The spectrograph is equipped with a Pixis 100B eXcelon ccd detector (pixel size 20×20 μm^2, 1340×100 pix, chip dimension 26.8×2 mm^2). The entrance slit was set to 50 μm and the discharge emission was projected on it by means of 6 m long, 1mm in diameter, fused silica optical fiber attached to the spectrograph utilizing an SMA connector. The discharge was focused on the fiber by a focusing lens with a focusing length of f=50 mm and an aperture of 25 mm. The distances between the lens and the fiber and between the lens and the discharge were equal and set to 2f=100 mm. The spectroscopic system was wavelength and intensity calibrated. Wavelength calibration, that includes also the resolution calibration, was performed using Cd and He lamps. With the grating of 1800 g/mm and 50 μm, the system gives a pure Gaussian instrumental profile with the full widths at half maximum that depend on the observed wavelength and are in range of 0.048 nm and 0.07 nm, respectively. The instrumental profiles for the UV adopted gratings are a bit asymmetric, therefore for the analysis of the line shapes, only profiles recorded by the use of the grating with 1800 g/mm have been used. The relative sensitivity of the spectroscopic system was determined using an integrating sphere. Such a spectroscopic system does not allow to acquire temporally resolved measurements and limits spatially resolved studies. For a rough spatial separation of discharge zones, two 0.5 mm wide and 1 cm high slits were positioned aligned along the 5 cm distance between the lens and the discharge, see Figure 1. This enabled separation of the emission from the hot discharge core and the periphery of the discharge where colder streamers were in contact with the treated liquid. Spectra were recorded using the "Step and Glue" function of the WinSpec32 software with typical exposure times of 5-10 s per window and with one accumulation.

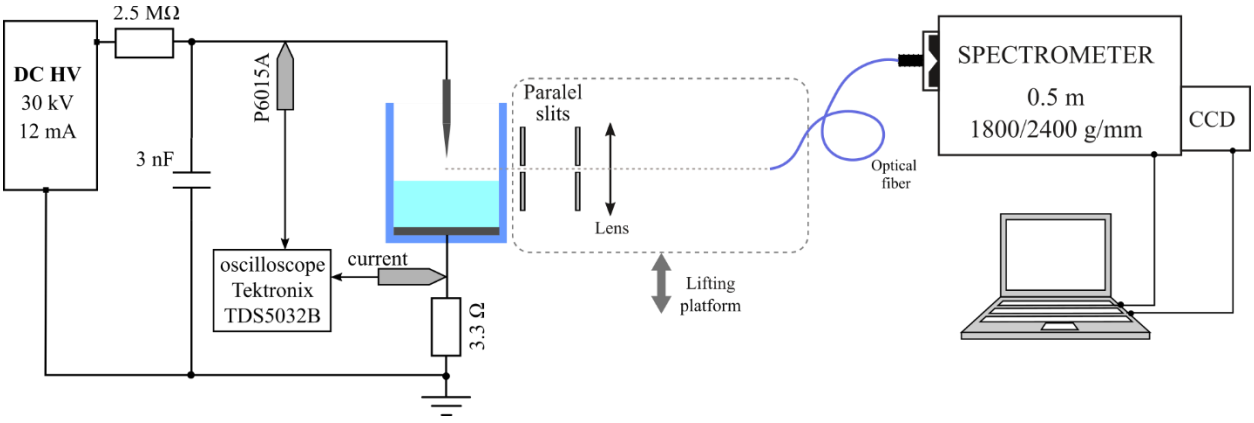

Figure 1. Experimental setup: schematics of the discharge cell, and of electrical and spectroscopic measurements.

RESULTS AND DISCUSSION

Electrical properties of the self-pulsing discharge are presented in Figure 2. When the applied voltage reaches the breakdown value, discharge occurs and the energy stored in the capacitor dissipates through the electrodes, which act as spark-gap switch, in several microseconds. Typical power of the discharge is in the range of a few wats to 20 W, depending on the experimental conditions. The obtained electrical properties and the discharge appearance itself are similar to those of the transient spark discharge.[25,26]

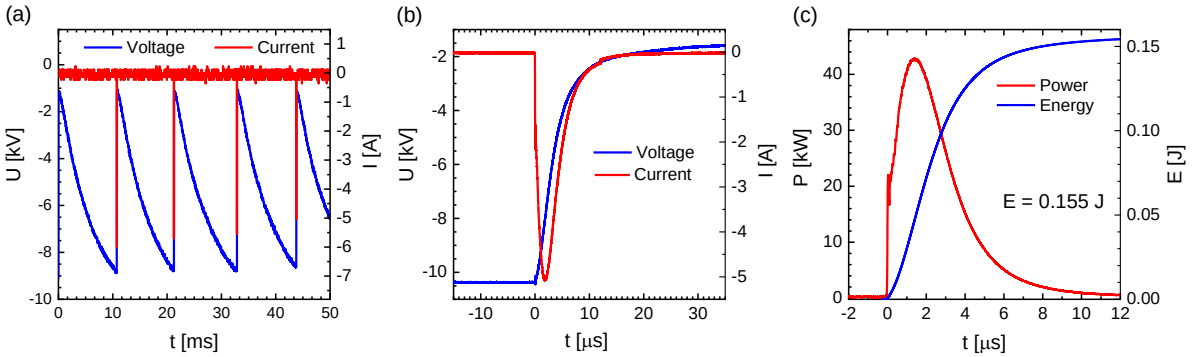

Figure 2. Electrical properties of the self-pulsing discharge: (a) voltage and current of multiple pulses, (b) voltage and current signals of the single pulse and (c) power and energy of the single pulse. The results are obtained for discharge in synthetic air and Mill-Q water as liquid electrode.

Instrumental profile of the spectrometer at a single wavelength and for the selected slit width of 50 μm is presented in Figure 3. It shows perfect Gaussian profile and enables deep analysis of the obtained line shapes emitted by the discharge. As mentioned before, we performed in this study spectroscopic measurements under all the experimental conditions we had tested in our previous work on PFOA degradation.[13] Typical PFOA treatment time was 30 minutes and typical acquisition time for one spectrum was 5 minutes. Therefore, three spectra per degradation experiment were performed: one at the beginning of the treatment (between 0 and 5. minutes), a second one in the middle of the treatment (between 12. and 18. minute) and a third one at the end of the treatment experiment (between 25. and 30. minute). All spectra were recorded in the 300-900 nm range. The results of representative spectra are presented in Figure 4 and Figure ***5***. The recorded emissions originate from the intense cores of the discharges.

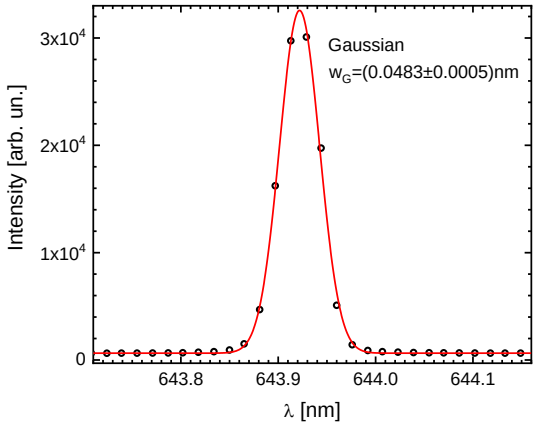

Figure 3. Typical instrumental profile of the spectrometer at 644 nm with an entrance slit width of 50 μm.

The discharge in air is dominated by nitrogen emission and by OH in the ultraviolet region, as expected. Besides, a very strong NH (A-X, 0-0) emission is detected at 336 nm, see Figure 4 (a). The NH is generated at high temperatures, in the order of several thousand kelvins, mainly through the reaction $N+H_2O \rightarrow OH+NH$ and it is often detected in the pulsed discharges in air above water surface [27]. Emission of atomic lines originating from the electrode material, such as Fe I and Cr I indicate development of high temperatures and sputtering of the cathode material. Emissions of three hydrogen lines, H_α, H_β and H_γ, are also recorded. Finally, numerous nitrogen and oxygen atomic lines are detected above 600 nm, see Figure 5 (a).

Emission of self-pulsing discharge in argon lacks signals due to nitrogen species which indicates that oxygen and hydrogen containing species originate from liquid i.e. water vapor. Figure 4 (b). OH emission is clearly detectable in argon discharge. Besides dominant production pathways through dissociative recombination of H_2O^+ or H_3O^+ [28,29], OH (A) can be produced in collisions of water molecules with argon metastables [30,31]. Cathode sputtering is also evident in the spectrum of argon discharge. Argon self-pulsing discharge in contact with liquid electrode also emits hydrogen Balmer series lines and argon and oxygen atomic lines, see Figure 5 (b).

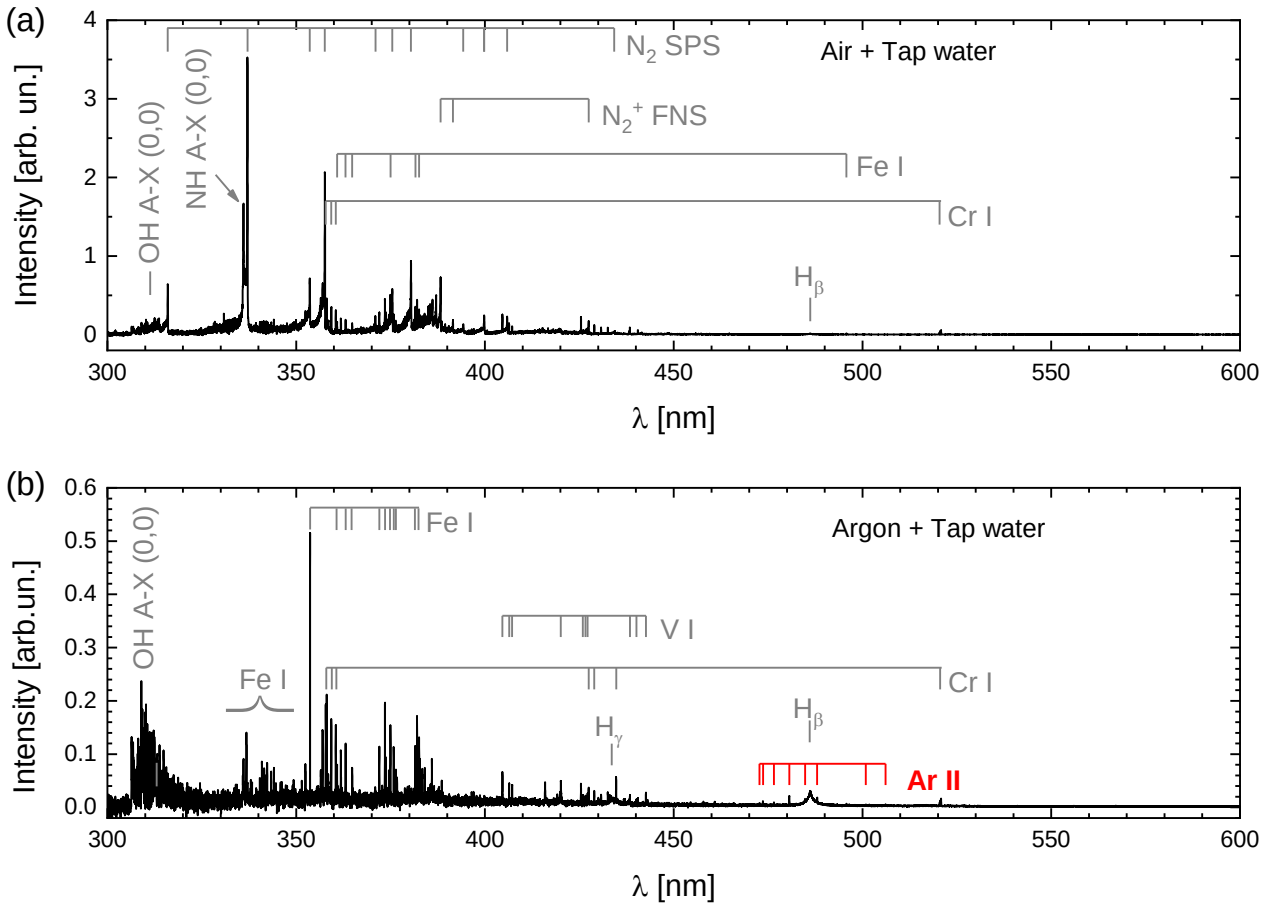

Figure 4. Typical spectra of the self-pulsing discharge recorded in the 300-600 nm range: (a) discharge in synthetic air in contact with tap water. (b) Discharge in argon in contact with tap water.

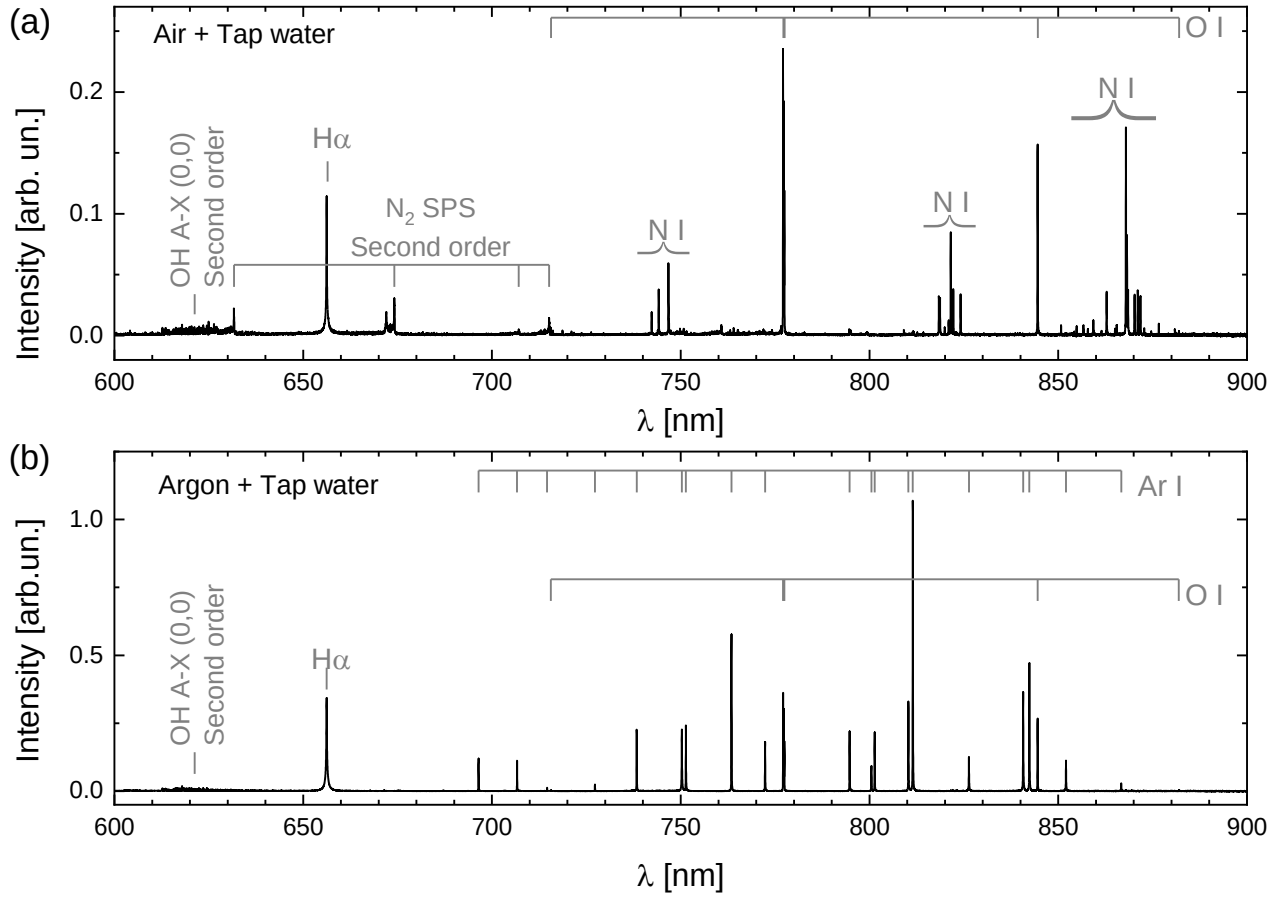

Figure 5: Typical spectra of the self-pulsing discharge recorded in the 600-900 nm range: (a) discharge in synthetic air in contact with tap water. (b) Discharge in argon in contact with tap water.

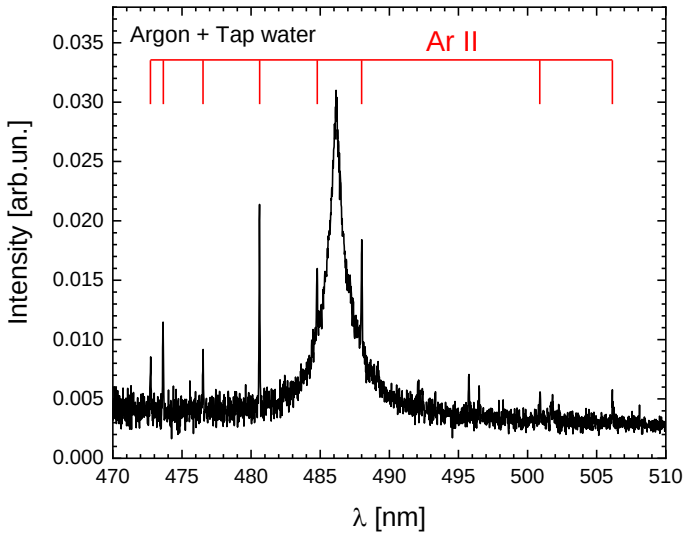

Figure 6. Argon ion lines emission around H_β line.I

Figure 6 documents the appearance of the argon ions emissions in the 472-507 nm range. Argon ion is the dominant ion during the discharge pulse. Ion/molecule reactions of Ar^+ with H_2O produce H_2O^+, OH and ArH^+. H_2O^+ in turn reacts with H_2O producing H_3O^+ and OH. It was shown previously that the density of argon ion follows the electron density behavior in the discharge including the absolute values. [32,33] The argon ion is of importance for the degradation of PFAS. It is assumed, that besides plasma and aqueous electrons, Ar ions are the main species responsible for PFAS attack initiating their degradation.[18]

Due to the current limiting influence of the liquid electrode, the expected pure spark nature of the observed discharge is indeed more complex and has not been extensively studied in the past from the physical point of view. The first studies showed single and particularly multichannel development of the discharge with a central core of the discharge and numerous branches developing from it in form of leaders and later streamers that touch the water surface.[34–39] Leaders were also observed in a surface barrier discharge emerging from a conductive water electrode.[40] In the present study, the emissions of the discharge core and of the leader/streamer periphery were recorded for self-pulsing discharge in air over water surface and are presented in Figure 7. The difference of the emission from the two regions is obvious. The lines corresponding to the electrode material are missing in the streamer phase, as expected, and the lines belonging to the nitrogen atomic emissions are less prominent in this region. The intensity of the observed NH band is much smaller. These observations encouraged further studies and comparison of two distinct discharge regions in air and argon discharge. Gas temperatures and electron densities were determined and compared to prove the assumptions based on the visual discharge appearance and observation of the overall emission spectra.

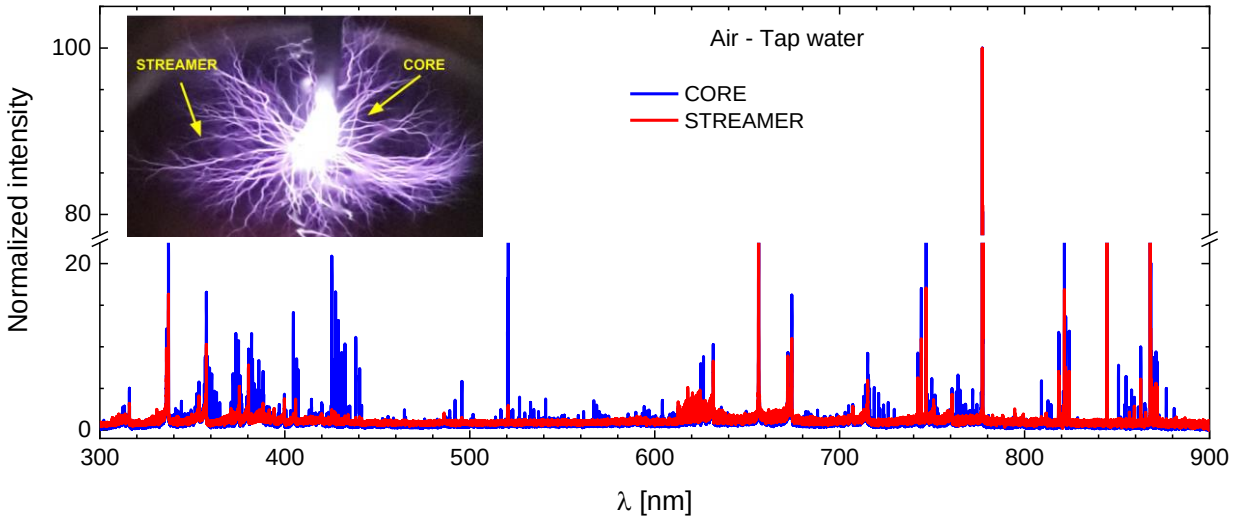

Figure 7. Comparison of two emission spectra emitted, respectively, from the central core of the self-pulsing discharge in air over water surface and its leader/streamer periphery. The photo of the discharge is presented in the inset of the figure with the marked recorded regions.

Gas temperatures are estimated under the assumption of thermalization of the excited molecules during their radiative lifetime due to the highly collisional nature of atmospheric

pressure plasma. Thus, the gas temperature can be identified with the rotational temperature of the selected molecules. For the discharge in air, the emission of the second positive nitrogen system is used to estimate the gas temperature, according to the conclusions presented in Ref. [41]. OH emission is used instead for the determination of the rotational temperature in argon discharge. The analysis of molecular optical emission spectra of the discharges to obtain rotational temperatures has been performed by means of MassiveOES software developed at Masaryk University in Brno [42–44].

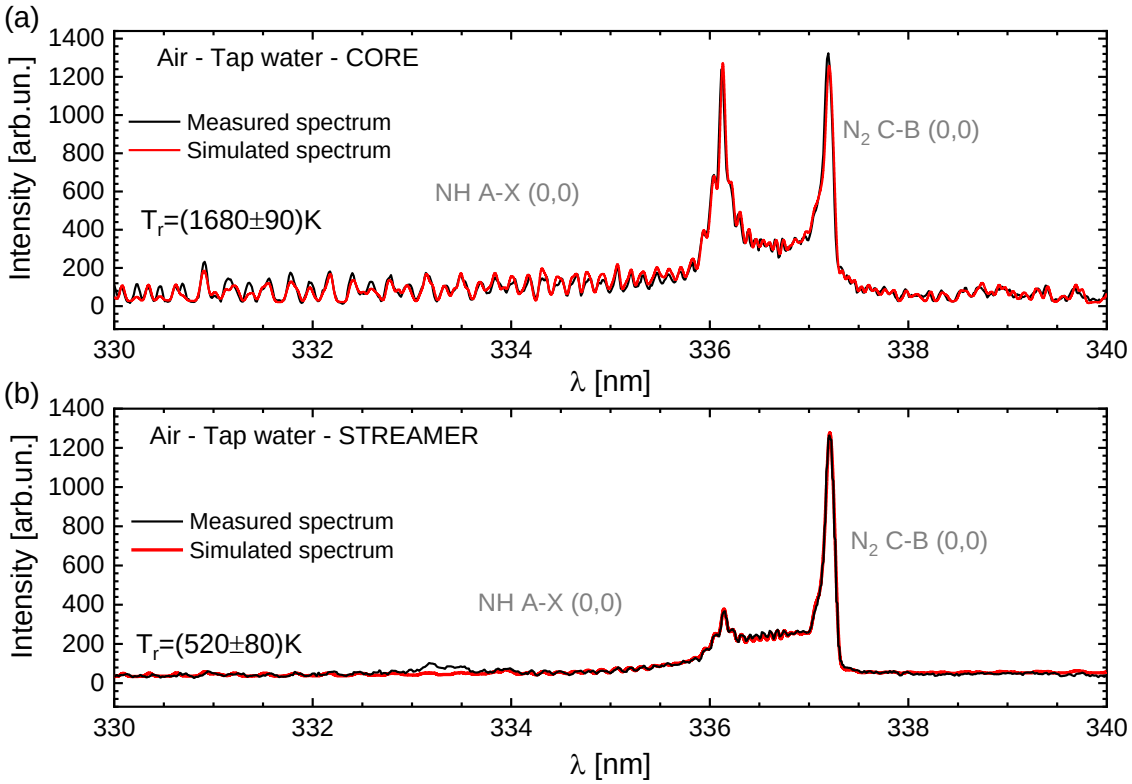

Figure 8. Measured and simulated spectra of N_2 C-B (0,0) and NH A-X (0,0) recorded from a bright discharge core (a) and from a leader/streamer periphery (b) of the self-pulsing discharge in synthetic air in contact with liquid sample.

As mentioned before, the gas temperature in air self-pulsing discharge was estimated by analysis of the second positive emission of molecular nitrogen. Being the most intense band, emission of the N_2 C-B (0,0) at 337.1 nm was selected and a sample of the analyzed results is presented in Figure 8. Although this emission overlaps with NH A-X (0,0) emission at 336.0 nm, it was nevertheless possible to perform satisfactory analysis with the used software. To be sure about the obtained results, the additional analysis of the nitrogen second positive system emission N_2 C-B (1,2) at 353.6 nm was also performed. The obtained results were in reasonable agreement and justified using the N_2 C-B (0,0) band. The temperatures obtained from the discharge core and the periphery of the discharge, which is in actual contact with the liquid, are significantly different. Namely, the temperature in the discharge core reaches 1700 K and reflects the sparking nature of the discharge, but as the discharge branches into leaders and further into streamers towards the water surface it drops to values around 500 K, much closer to those found regular streamers. The

obtained results are in accordance with the visible appearance of the discharge. By naked eye observation it was possible to detect differences in the spectra obtained, respectively, from the discharge core, close to the cathode, and the periphery, close to the water surface.

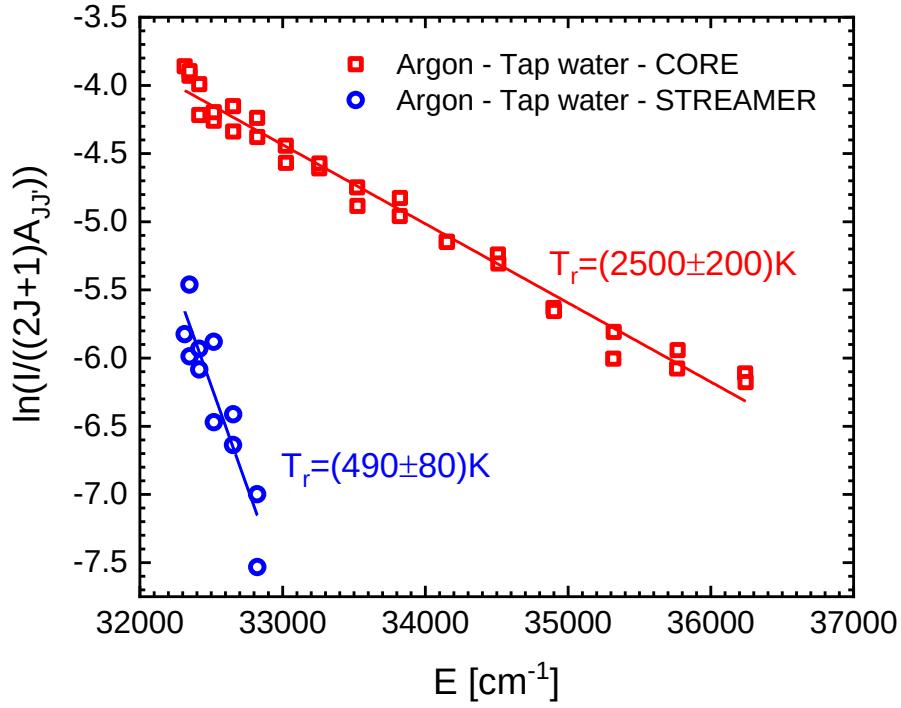

Figure 9. Two examples of OH A-X Boltzmann plot corresponding to the emission of the self-pulsing argon discharge in contact with water from the discharge core and from thr leader/streamer region.

The analysis of the OH emission in the discharges in contact with the liquid is a bit more complex because excited OH radicals in atomic gases, such as argon, and water vapor show significant overpopulation of high rotational states [45]. For higher levels the rotational distribution of molecules is influenced by the formation process even at atmospheric pressure and the temperature corresponding to the small rotational numbers of OH(*A*) can be used as an estimate of the gas temperature [30,45]. For this reason, OH A-X emission spectra has not been fitted, but only the lines with smaller rotational numbers were selected to build a Boltzmann plot for their intensity distribution. This procedure was possible by the use of the same software package MassiveOES mentioned earlier. The examples of two Boltzmann plots are presented in Figure 9. The obtained results are in qualitative accordance with the results for self-pulsing discharge in air giving temperatures of 2500 K in the discharge core and of about 500 K in the periphery of the discharge, respectively. Following the previously described procedures gas temperatures were estimated for all six combinations of working gases and liquids, at the beginning, in the middle and at the end of each experiment.

Electron densities were determined based on the analysis of Stark broadening of hydrogen H_α and H_β lines [46,47], following the well-defined routine procedures [48]. It is a known feature that

hydrogen lines, especially H_α may suffer from self-absorption. H_α line is the most intense hydrogen emission and from that point of view the best to use for the analysis. Therefore, the self-absorption test based on checking the line intensity ratios within the O I multiplet at 777 nm was performed. If a reduction in the observed intensity of the strongest line in the multiplet relative to that of a weaker one with respect to the known transition probabilities occurs, then self-absorption is present [48]. In all the experiments performed in this work, the ratio of the observed lines matched the ratio of the line strengths taken from the NIST Atomic Spectra Database [49]. Additional check of the validity of the obtained results is certainly provided by comparison of the values of the electron density determined using both hydrogen lines. Beside the self-absorption test, determination of relevant spectral line broadening mechanisms is of the highest importance to support the results. As mentioned before, instrumental line profiles were obtained for the whole wavelength range. They showed Gaussian structure with full widths at half maximum, also known as halfwidths, of w_I=0.060 nm at 480 nm and w_I=0.048 nm at 643 nm, respectively, which are the closest Cd lines to the observed hydrogen lines. Having in mind substantial gas temperatures for some experimental conditions, not negligible Doppler broadening, $w_{D,}$ of hydrogen lines was calculated, and its contribution to the overall Gaussian halfwidth, w_G, was incorporated using the formula $w_G = \sqrt{(w_I^2 + w_D^2)}$. Since the discharges were operated at the atmospheric pressures, the pressure broadening, in particular the van der Waals broadening of hydrogen lines in air and argon, was evaluated and its contribution, $w_{VdW,}$ was subtracted from the overall Lorentzian halfwidth. Lorentzian halfwidth, w_L, was obtained by Voigt fit of the experimental profile with the predefined w_G. Finally, Stark full width at half of the peak maximum was calculated as $w_S = w_L - w_{VdW}$. The determined instrumental, Doppler and van der Waals broadening contributions to the overall line width are shown in Figure 10.

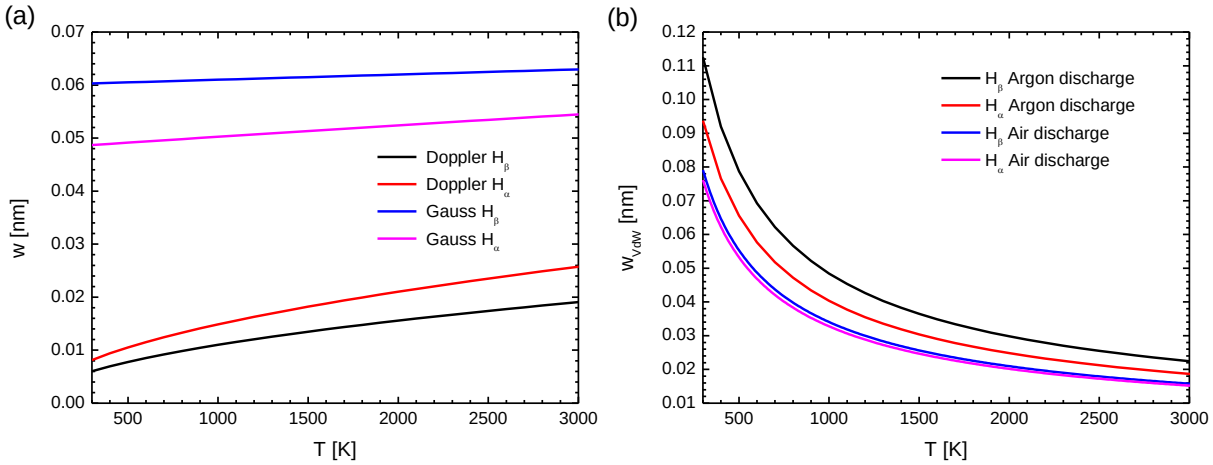

Figure 10: Determined Doppler broadening and overall Gaussian halfwidths of hydrogen lines (a) and van der Waals broadening Lorentzian halfwidths of hydrogen lines in argon and in air (b).

Thanks to the in line positioned slits in front of the projection lens, the emissions from different discharge regions could be roughly separated. Thus, we were able to separate hydrogen line profiles emitted from the discharge core and from the leader/streamer region, respectively. The difference between the obtained H_α profiles is evident in Figure 11. The line profile emitted from

the discharge core is much broader and even slightly shifted to the red, which implies much higher electron density in the discharge core, which is in line with the results of the discharge temperature estimate. Hydrogen line profiles were further analyzed quantitively in detail. Electron densities were calculated using the formulas given in Ref. 47. Examples of hydrogen lines emitted from air and argon self-pulsing discharges in contact with liquid are presented in Figure 12. Hydrogen line profiles emitted from the core are complex and could not be fitted by a single Voigt profile. The complex structures of the emitted lines may arise from a nonhomogeneous discharge structure in space and time as well as from and time and space unresolved measurements. Both mentioned factors may be responsible for the line profiles obtained in the presented study. Namely, the discharge is pulsed, so it changes in time. It consists of a bright core and surrounding leaders and streamers which propagate towards the water surface and the periphery. The use of an optical fiber significantly limits the possibility of spatially resolved measurements and the used ccd detector could not be used for the temporally resolved measurements. Consequently, the line profiles emitted from the the discharge core were fitted with two Voigt function profiles, in a similar way as presented in Refs. 40,50. The examples of the two Voight functions fitted line profiles are presented in Figure 12 (a), (c) and (f). The line profiles consist of a wide component that reflects high electron density and of a narrow one with one order of magnitude lower electron concentration. The first assumption is that the wide line components originate from the discharge region close to the high voltage electrode, i.e. the cathode, and that the narrow line components are emitted from the part where the discharge core starts to branch into the leaders and streamers.

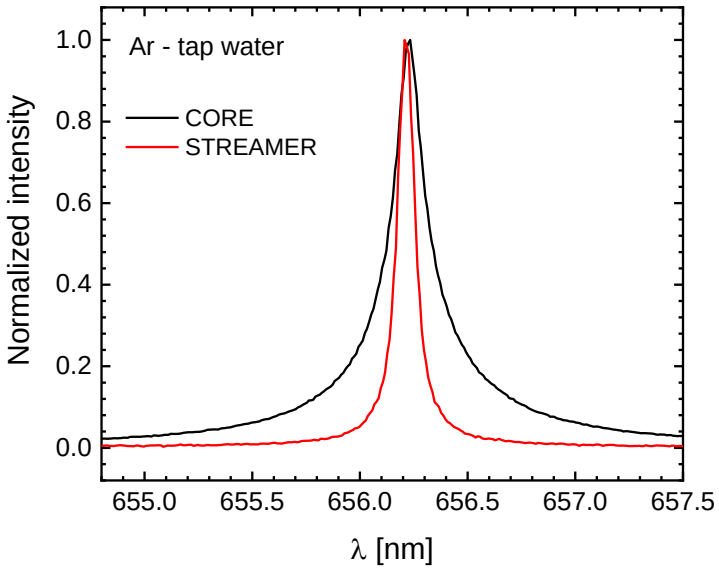

Figure 11. Comparison of the normalized profiles Hydrogen Balmer alpha line emitted by two regions of the self-pulsing discharge in argon.

The analysis of hydrogen Balmer alpha line profiles emitted from the discharge core close to the high voltage electrode gives two electron densities, both for air and argon, see Figure 12 (a) and (c). The higher electron densities are in the order of 10^{16} cm^{-3}, and can reach the level of 10^{17} cm^{-3}, which reflects the sparking nature of the discharge. Interestingly, the electron density values don't differ much for different working gases, if other parameters are the same. That is even more pronounced for the electron densities obtained with narrow line components where the values of the electron density are in the order of 10^{15} cm^{-3}. The results obtained with more intense hydrogen alpha line were confirmed by the analysis of the hydrogen Balmer beta line presented in Figure 12 (f). Both lines were analyzed for all experiments for which the Balmer beta line was visible. As can be seen, the matching of the results obtained with the two hydrogen lines is complete.

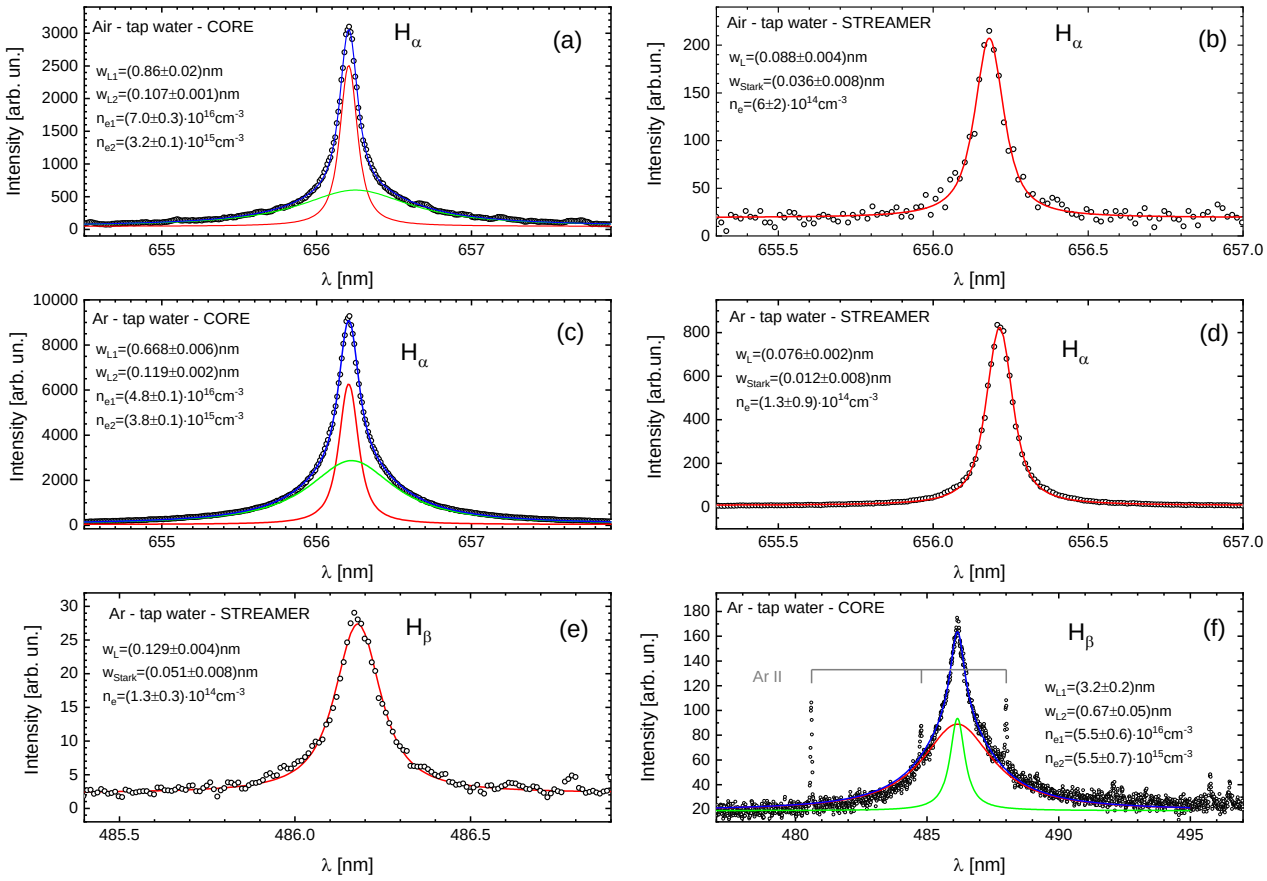

Figure 12. Examples of the hydrogen lines profiles for different experimental conditions: Hydrogen Balmer alpha line emitted from the core of the self-pulsing discharge in air (a); Hydrogen Balmer alpha line emitted from the leader/streamer region of the self-pulsing discharge in air (b); Hydrogen Balmer alpha line emitted from the core of the self-pulsing discharge in argon (c); Hydrogen Balmer alpha line emitted from the leader/streamer region of the self-pulsing discharge in argon (d); Hydrogen Balmer beta line emitted from the leader/streamer region of the self-pulsing discharge in argon (e);); Hydrogen Balmer beta line emitted from the core of the self-pulsing discharge in argon (f).

Similarly to the discharge core, the emission of the hydrogen lines from the periphery of the discharge was also recorded. Examples of the obtained line profiles are presented in Figure 12 (b), (d) and (e). The electron densities of 10^{14} cm^{-3} obtained from the discharge periphery confirmed streamer properties of the discharge in close contact with the liquid. Determination of the electron density using hydrogen Balmer alpha line are on the lower limit of the method [47], therefore confirmation with the analysis of hydrogen Balmer beta line was necessary. In this case too, comparison of the electron densities obtained by two hydrogen lines showed excellent matching. It is worth mentioning that at lower gas temperatures, as is the case in the streamers observed in our experiments (about 500 K), Van der Waals broadening plays an important role and has to be taken into account. For the emission from the discharge core, the temperatures are typically above 1500 K and the lines are much more broadened by the Stark effect. Thus, not taking into account the contribution of the Van der Waals broadening does not affect the results significantly, but reduces the errors. Furthermore, for the determination of the electron density based on the narrow component in the two-fit method and for the determination of the Van der Waals broadening, the same temperature was taken as in the case of the broad component. If we assume that this component comes from the leader emission, a lower gas temperature should be taken which would result in a lower electron density. This temperature was not estimated. However, if one assumes the lowest possible leader temperature to be equal to the streamer temperature, e.g. about 500 K, the obtained values of the electron density would be reduced by a factor of two in the worst case.

In conclusion, from the analysis of the hydrogen lines profiles one can deduce that the electron density decreases as the discharge branches towards the liquid surface, a conclusion which is in accordance with the photo shown in the inset of Figure 7. Having in mind the properties of spark, leader and streamer discharges it is reasonable to attribute three different values of the electron density to these discharge operation modes.

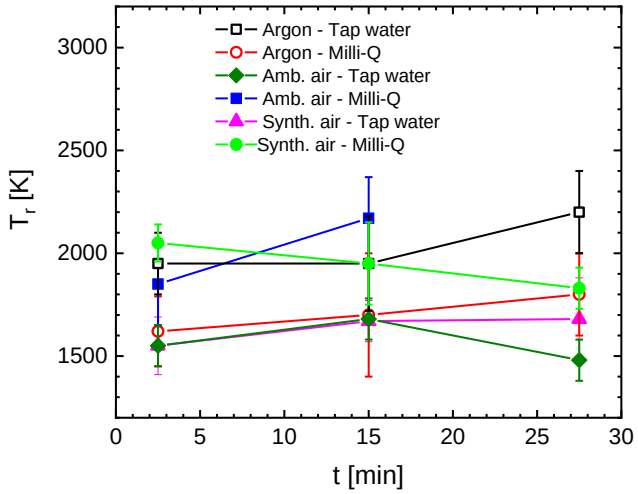

Figure 13. Development of the rotational temperatures in the discharge core during the degradation experiments for all examined conditions.

The overall results of the rotational, i.e. gas temperature values for all experiments are presented in Figure 13. The temperatures during each degradation experiment remain the same within the estimated measurements errors. All temperatures in the discharge core are in the 1500-2200 K range. It should be noted here that the temperatures in the periphery of the discharge behave similarly for all experiments and that they are about 500 K. If one compares different discharge conditions in the discharge core, one can note that discharges in air behave similarly, namely synthetic and ambient air discharges in contact with tap water give almost the same temperature behavior. A similar trend is observed for both air discharges in contact with Milli-Q water, just the values are slightly higher. Interestingly, the situation with argon discharges is opposite, the higher temperatures are obtained with tap water.

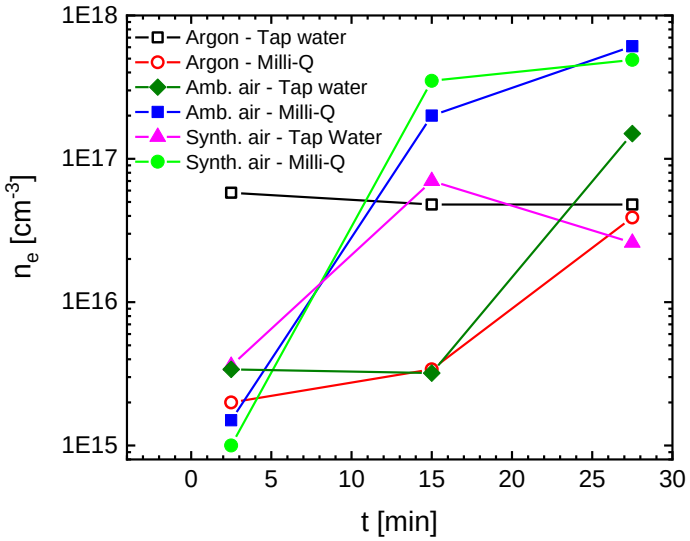

Figure 14. Development in time of the electron densities in the discharge core during degradation experiments under all examined conditions.

Electron density development curves for all experiments are shown in Figure 14. The first impression is that for most of the experiments the electron density in the discharge core, close to the cathode, rises during the treatment time. The observed changes in the electron density may be as large as two orders of magnitude. The only stable results are obtained for the argon discharge in contact with tap water. Beside this experiment, the smallest change during the applied treatment time of 30 min is obtained for argon self-pulsing discharge in contact with Milli-Q water. The presented electron density distributions are in fact the electron density numbers obtained with the wide hydrogen lines component. The results of the narrow component are not presented here, but they show similar behavior. Similar to the temperature results, electron density measured at the discharge periphery is in the order of 10^{14} cm^{-3} for all experiments.

The obtained results of the electron density are proportional to the discharge current which depends on the conductivity of the liquid. Thus, the results of the electron density cannot be discussed without the insight in the change of the liquid conductivity during the degradation

experiments, see Figure 15. Comparing the data in Figure 14 and Figure 15, it is obvious that high electron densities could not be achieved when the liquid conductivity was low, as is the case in Milli-Q water before treatment (time zero). Thus, the obtained initial values of the electron density for all gasses are between 1 and $2 \cdot 10^{15}$ cm^{-3}. It is known that discharges in air produce nitrogen oxides which in water form nitric acid. Acid dissociation leads to a pH reduction and to an increase in the liquid conductivity in Milli-Q water. In turn, an increase in conductivity causes an increase in the current amplitude and reduces the current pulse which enables higher peak electron densities [13]. This effect enables rapid increase of the electron density during the PFOA degradation experiment and the achievement of the remarkable electron density values of $6 \cdot 10^{17}$ cm^{-3} for air discharge in contact with Milli-Q water. In contrast, the natural carbonates present in tap water neutralize the hydronium ions produced by air discharges and limit the increase of the conductivity. Therefore, the final conductivities of Milli-Q solutions treated with discharges in air reach the highest values which enable discharge pulses with the highest electron density.

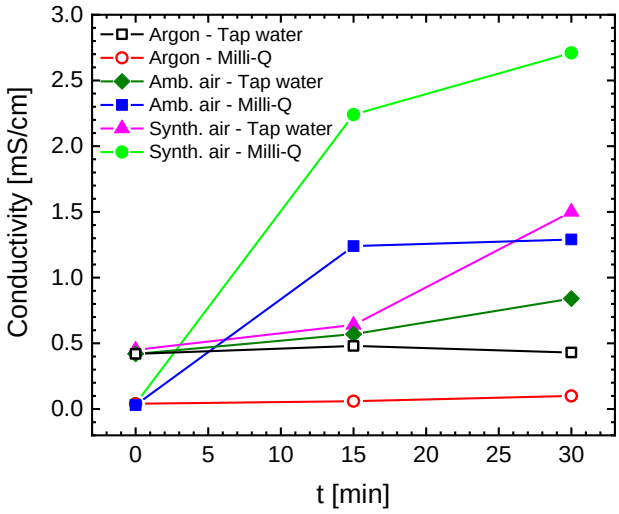

Figure 15. Changes of the conductivity of the treated liquid during the discharge treatment experiments for all examined conditions.[13]

High electron density was shown to be favorable for the PFOA degradation, but in most of the discharges it changes from very low values and reaches maximum as the conductivity increases.[13] In contrast, argon discharge in contact with tap water operates with high electron density at the beginning of the process which is about $6 \cdot 10^{16}$ cm^{-3} and remains almost constant until the end of the experiment. High electron density in argon discharge with tap water may be the main reason for the most effective degradation process of PFOA[13] for two reasons. First, the electron density is proportional to the argon ion density [32,33] and second may be favorable for the solvation of the electrons in the liquid [51].

CONCLUSION

The article presents the results of a spectroscopic study of the self-pulsing discharge, previously developed and successfully used for the degradation of PFAS in aqueous solutions. The

results show the complex nature of this type of discharge which is influenced mainly by the liquid electrode. The electrical properties imply a sparking nature of the discharge, but its visual appearance shows that the discharge starts as a bright and hot phenomenon that occurs close to the high voltage electrode, the cathode, and then separates into many leaders that finally branch into numerous streamers that spread over the entire liquid surface. These observations are supported and rationalized by the spectroscopic measurements that allow to distinguish several regions with different gas temperatures and electron densities. In the core plasma, close to the cathode, temperatures reach 2500 K and electron densities range from 10^{16} to 10^{17} cm^{-3}. In going further away from the cathode, these values decrease, with the electron density falling down by one order of magnitude. Finally, close to the liquid surface, where streamers dominate, the electron density drops to the 10^{14} cm^{-3} range and the gas temperature to ~500 K. Thus, the discharge investigated in this study consists of a range of different plasma regimes, which further entangle already complex interplay of plasma and liquid. This article reveals just a part of this complexity and opens space for further and more detailed spatio-temporally resolved investigations supported by modeling.

Acknowledgements

The authors gratefully acknowledge financial support from Regione Veneto (POR FSE 2014-2020, DGR. 11 del 05/01/2018) for the project "WaterPLAS", Grant n. 2105-43-11-2018, and from the University of Padova (P-DiSC#06BIRD2019-UNIPD).

AIP Publishing Data Sharing Policy

The data that support the findings of this study are available from the corresponding author upon reasonable request.

References

[1] P.J. Bruggeman, M.J. Kushner, B.R. Locke, J.G.E. Gardeniers, W.G. Graham, D.B. Graves, R.C.H.M. Hofman-Caris, D. Maric, J.P. Reid, E. Ceriani, D. Fernandez Rivas, J.E. Foster, S.C. Garrick, Y. Gorbanev, S. Hamaguchi, F. Iza, H. Jablonowski, E. Klimova, J. Kolb, F. Krcma, P. Lukes, Z. Machala, I. Marinov, D. Mariotti, S. Mededovic Thagard, D. Minakata, E.C. Neyts, J. Pawlat, Z.L. Petrovic, R. Pflieger, S. Reuter, D.C. Schram, S. Schröter, M. Shiraiwa, B. Tarabová, P.A. Tsai, J.R.R. Verlet, T. von Woedtke, K.R. Wilson, K. Yasui, and G. Zvereva, Plasma Sources Sci. Technol. **25**, 053002 (2016).

[2] P. Bruggeman and C. Leys, J. Phys. D. Appl. Phys. **42**, 053001 (2009).

[3] B.P. Dojčinović, G.M. Roglić, B.M. Obradović, M.M. Kuraica, M.M. Kostić, J. Nešić, and D.D. Manojlović, J. Hazard. Mater. **192**, 763 (2011).

[4] B.M. Cadorin, V.D. Tralli, E. Ceriani, L.O. de B. Benetoli, E. Marotta, C. Ceretta, N.A. Debacher, and C. Paradisi, J. Hazard. Mater. **300**, 754 (2015).

[5] D. Manojlovic, D.R. Ostojic, B.M. Obradovic, M.M. Kuraica, V.D. Krsmanovic, and J. Puric, Desalination **213**, 116 (2007).

[6] E. Marotta, E. Ceriani, M. Schiorlin, C. Ceretta, and C. Paradisi, Water Res. **46**, 6239 (2012).

[7] M. Magureanu, D. Piroi, N.B. Mandache, V. David, A. Medvedovici, C. Bradu, and V.I. Parvulescu, Water Res. **45**, 3407 (2011).

[8] M. Marković, M. Jović, D. Stanković, V. Kovačević, G. Roglić, G. Gojgić-Cvijović, and D. Manojlović, Sci. Total Environ. **505**, 1148 (2015).

[9] M.S. Jović, B.P. Dojčinović, V. V. Kovačević, B.M. Obradović, M.M. Kuraica, U.M. Gašić, and G.M. Roglić, Chem. Eng. J. **248**, 63 (2014).

[10] A. Giardina, F. Tampieri, O. Biondo, E. Marotta, and C. Paradisi, Chem. Eng. J. **372**, 171 (2019).

[11] K. Oehmigen, M. Hähnel, R. Brandenburg, C. Wilke, K.-D. Weltmann, and T. von Woedtke, Plasma Process. Polym. **7**, 250 (2010).

[12] R.C. Buck, J. Franklin, U. Berger, J.M. Conder, I.T. Cousins, P. de Voogt, A.A. Jensen, K. Kannan, S.A. Mabury, and S.P.J. van Leeuwen, Integr. Environ. Assess. Manag. **7**, 513 (2011).

[13] M. Saleem, O. Biondo, G. Sretenović, G. Tomei, M. Magarotto, D. Pavarin, E. Marotta, and C. Paradisi, Chem. Eng. J. **382**, 123031 (2020).

[14] R. Hayashi, H. Obo, N. Takeuchi, and K. Yasuoka, Electr. Eng. Japan **190**, 9 (2015).

[15] H. Obo, N. Takeuchi, and K. Yasuoka, Int. J. Plasma Environ. Sci. Technol. **9**, 62 (2015).

[16] G.R. Stratton, F. Dai, C.L. Bellona, T.M. Holsen, E.R. V. Dickenson, and S. Mededovic Thagard, Environ. Sci. Technol. **51**, 1643 (2017).

[17] V. Jovicic, M. Khan, A. Zbogar-Rasic, N. Fedorova, A. Poser, P. Swoboda, and A. Delgado, Energies **11**, 1290 (2018).

[18] R.K. Singh, S. Fernando, S.F. Baygi, N. Multari, S.M. Thagard, and T.M. Holsen, Environ. Sci. Technol. **53**, 2731 (2019).

[19] R.K.M. Bulusu, R.J. Wandell, Z. Zhang, M. Farahani, Y. Tang, and B.R. Locke, Plasma Process. Polym. **17**, 2000074 (2020).

[20] A.J. Lewis, T. Joyce, M. Hadaya, F. Ebrahimi, I. Dragiev, N. Giardetti, J. Yang, G. Fridman, A. Rabinovich, A.A. Fridman, E.R. McKenzie, and C.M. Sales, Environ. Sci. Water Res. Technol. **6**, 1044 (2020).

[21] B.S. Crimmins, X. Xia, P.K. Hopke, and T.M. Holsen, Anal. Bioanal. Chem. **406**, 1471 (2014).

[22] R. Lewis, L. Johns, and J. Meeker, Int. J. Environ. Res. Public Health **12**, 6098 (2015).

[23] N.M. Crawford, S.E. Fenton, M. Strynar, E.P. Hines, D.A. Pritchard, and A.Z. Steiner, Reprod. Toxicol. **69**, 53 (2017).

[24] J.L. Domingo and M. Nadal, J. Agric. Food Chem. **65**, 533 (2017).

[25] M. Janda, V. Martišovitš, K. Hensel, L. Dvonč, and Z. Machala, Plasma Sources Sci. Technol. **23**, 065016 (2014).

[26] M. Janda, T. Hoder, A. Sarani, R. Brandenburg, and Z. Machala, Plasma Sources Sci. Technol. **26**, 055010 (2017).

[27] P. Bruggeman, J.L. Walsh, D.C. Schram, C. Leys, and M.G. Kong, Plasma Sources Sci. Technol. **18**, 045023 (2009).

[28] P. Bruggeman, F. Iza, P. Guns, D. Lauwers, M.G. Kong, Y.A. Gonzalvo, C. Leys, and D.C. Schram, Plasma Sources Sci. Technol. **19**, 015016 (2010).

[29] J.Y. Park, P. V Kostyuk, S.B. Han, J.S. Kim, C.N. Vu, and H.W. Lee, J. Phys. D. Appl. Phys. **39**, 3805 (2006).

[30] T. Verreycken, D.C. Schram, C. Leys, and P. Bruggeman, Plasma Sources Sci. Technol. **19**, 045004 (2010).

[31] V. V Kovačević, B.P. Dojčinović, M. Jović, G.M. Roglić, B.M. Obradović, and M.M. Kuraica, J. Phys. D. Appl. Phys. **50**, 155205 (2017).

[32] Y. Luo, A.M. Lietz, S. Yatom, M.J. Kushner, and P.J. Bruggeman, J. Phys. D. Appl. Phys. **52**, 044003 (2019).

[33] W. Van Gaens and A. Bogaerts, J. Phys. D. Appl. Phys. **46**, 275201 (2013).

[34] V.P. Belosheev, Tech. Phys. **43**, 1329 (1998).

[35] V.P. Belosheev, Tech. Phys. **43**, 783 (1998).

[36] V.P. Belosheev, Tech. Phys. **44**, 381 (1999).

[37] V.P. Belosheev, Tech. Phys. **45**, 922 (2000).

[38] A.F. Aleksandrov, D.N. Vaulin, A.P. Ershov, and V.A. Chernikov, Moscow Univ. Phys. Bull. **64**, 100 (2009).

[39] A.F. Aleksandrov, D.N. Vaulin, R. Qi, and V.A. Chernikov, Moscow Univ. Phys. Bull. **67**, 312 (2012).

[40] N. Cvetanović, O. Galmiz, P. Synek, M. Zemánek, A. Brablec, and T. Hoder, Plasma Sources Sci. Technol. **27**, 025002 (2018).

[41] A.N. Goyette, J.R. Peck, Y. Matsuda, L.W. Anderson, and J.E. Lawler, J. Phys. D. Appl. Phys. **31**, 1556 (1998).

[42] J. Voráč, P. Synek, L. Potočňáková, J. Hnilica, and V. Kudrle, Plasma Sources Sci. Technol. **26**, 025010 (2017).

[43] J. Voráč, P. Synek, V. Procházka, and T. Hoder, J. Phys. D. Appl. Phys. **50**, 294002 (2017).

[44] J. Voráč, L. Kusýn, and P. Synek, Rev. Sci. Instrum. **90**, 123102 (2019).

[45] P. Bruggeman, D.C. Schram, M.G. Kong, and C. Leys, Plasma Process. Polym. **6**, 751 (2009).

[46] M.A. Gigosos, M.Á. González, and V. Cardeñoso, Spectrochim. Acta Part B At. Spectrosc. **58**, 1489 (2003).

[47] N. Konjević, M. Ivković, and N. Sakan, Spectrochim. Acta Part B At. Spectrosc. **76**, 16 (2012).

[48] N. Konjević, Phys. Rep. **316**, 339 (1999).

[49] A. Kramida, Y. Ralchenko, J. Reader, and N.A. Team, Natl. Inst. Stand. Technol. Gaithersburg, MD. (2020).

[50] J. Jovović, S. Stojadinović, N.M. Šišović, and N. Konjević, Surf. Coatings Technol. **206**, 24 (2011).

[51] P. Rumbach, D.M. Bartels, R.M. Sankaran, and D.B. Go, Nat. Commun. **6**, 1 (2015).